Vibrational dynamics of myoglobin determined by the phonon-assisted Mössbauer effect

K. Achterhold,[1] C. Keppler,[1] A. Ostermann,[1] U. van Bürck,[2] W. Sturhahn,[3] E. E. Alp,[3] and F. G. Parak[1,*]
[1]*Physik-Department E17, Technische Universität München, 85747 Garching, Germany*
[2]*Physik-Department E13, Technische Universität München, 85747 Garching, Germany*
[3]*Advanced Photon Source, Argonne National Laboratory, Argonne, Illinois 60439*
(Received 9 July 2001; published 17 May 2002)

The phonon-assisted Mössbauer effect is used to determine the partial phonon density of states of the iron within the active center of deoxymyoglobin, carboxymyoglobin, and dry and wet metmyoglobin between 40 and 300 K. Between 0 and 1 meV the iron density of states increases quadratically with the energy, as in a Debye solid. Mean sound velocities are extracted from this slope. Between 1 and 3 meV a nearly quadratic ''Debye-like'' increase follows due to the similar strength of intermolecular and intramolecular forces. Above 3 meV, optical vibrations are characteristic for the iron-ligand conformation. The overall mean square displacements of the heme iron atom obtained from the density of states agree well with the values of Mössbauer absorption experiments below 180 K. In the physiological temperature regime the data confirm the existence of harmonic vibrations in addition to the protein specific dynamics measured by Mössbauer absorption. In the Debye energy regime the mean square displacement of the iron is in agreement with that of the hydrogens measured by incoherent neutron scattering demonstrating the global character of these modes. At higher energies the vibration of the heavy iron atom at 33 meV in metmyoglobin is as large as that of the lightweight hydrogens at that energy. A freeze dried, rehydrated ($h=0.38$ g H_2O/g protein) metmyoglobin sample shows an excess of states above the Debye law between 1 and 3 meV, similar to neutron scattering experiments. The room temperature density of states below 3 meV exhibit an increase of the density compared to the low temperature data, which can be interpreted as mode softening.

DOI: 10.1103/PhysRevE.65.051916 PACS number(s): 87.14.Ee, 87.15.−v, 87.64.−t

INTRODUCTION

Textbooks of solid state physics begin with an introduction to structure and dynamics. A detailed description of crystals containing only a few number of atoms in the unit cell is given. Several complications arise if the periodicity of a crystal is given up. The complexity of problems increases also by investigating the condensed matter consisting of rather large molecules such as proteins. Nevertheless, the x-ray structure determination of proteins has been possible since several decades. In 1960, the structure of myoglobin (Mb), an oxygen-storing protein, was solved by Kendrew *et al.* [1]. From this time on Mb became a key molecule for the development of new methods for the investigation of proteins and the study of protein dynamics. A further progress was obtained by the determination of the individual mean square displacements $\langle x^2 \rangle$ of the atoms of a protein [2]. The flexibility of protein molecules differs along the chain. In order to distinguish static and dynamic displacements of the atoms, the temperature dependence of the mean square displacements has been investigated. Going to very low temperatures, the $\langle x^2 \rangle$ values do not approach the classical value of zero [3]. The remaining structural disorder indicates the existence of conformational substates as demanded by flash photolysis experiments on carboxymyoglobin (MbCO) [4]. Only recently it became possible to distinguish intramolecular and intermolecular motions in Mb crystals by the normal mode refinement of the x-ray data of metmyoglobin [5,6].

X-ray structure determinations allowed also to analyze intermediate states between stable conformations of metmyoglobin (Mbmet) [7–10]. Recently it became possible to follow structural changes of MbCO after photolysis of CO in real time by time resolved x-ray structure analysis [11].

Early hints for a physical understanding of protein dynamics came from Mössbauer absorption spectroscopy on ^{57}Fe. This method labels motions coupled to the iron atom occurring on a time scale faster than 100 ns. Coming from very low temperatures, the $\langle x^2 \rangle$ value at the iron atom increases linearly with temperature. At about 180 K a much stronger increase of $\langle x^2 \rangle$ starts, indicating that a new channel of motions becomes available [12–14]. Similar results were obtained by incoherent neutron scattering [15].

Besides the huge number of experiments, theoretical investigations have been performed (compare also [16–18]). Theoretical tools such as molecular dynamic simulations [17,19,20] and normal mode analysis [16,21] have been developed to yield further information on atomic motions. The normal mode analysis was lately used to investigate the intramolecular vibrations of Mb [22].

Nevertheless, a clear physical picture of protein dynamics is still missing, even in case of Mb. Mössbauer effect with synchrotron radiation offers a new tool to investigate physical details [23]. Employing coherent scattering, the method of nuclear forward scattering of synchrotron radiation [24] has been used for experiments on myoglobin [25]. In incoherent scattering, the phonon-assisted Mössbauer effect allows to get information on intramolecular vibrations in the meV regime [26,27]. The first inelastic scattering spectra of phonons coupling to the Mössbauer isotope ^{57}Fe within Mb were reported by Keppler *et al.* [28] and recently by Sage

*Author to whom correspondence should be addressed.

et al. [29] but no density of phonon states was extracted from the data. In the following we report experiments performed at the European Synchrotron Radiation Facility (ESRF) in Grenoble and the Advanced Photon Source (APS) in Argonne using the phonon-assisted Mössbauer effect in Mb. The investigations have been carried out in a large temperature regime in order to study the vibrational modes coupling to a metal center in a protein.

MATERIALS AND METHOD

Sperm whale myoglobin was used for the experiments. For the enrichment of the protein with the Mössbauer isotope ^{57}Fe the heme was extracted with 2-butanone at *p*H 2.3. The recombination with ^{57}Fe heme was done according to [30]. The myoglobin solution was purified using a cation exchange chromatography column (sp-sepharose) on a Pharmacia fast performance liquid chromatograph (FPLC). The crystals were grown with the batch method from a solution of 3.2M $(NH_4)_2SO_4$ and 50 mM sodium phosphate at *p*H 6.8 containing 30-mg/ml myoglobin. The crystals belong to the space group $P2_1$ and were reduced by sodium dithionite, enlarging its concentration stepwise to a 20-fold stoichiometric excess. The reduction and filling into a vacuum tight plastic sample holder was done under an argon atmosphere. Superfluid buffer solution was removed to reduce absorption and to ensure a high amount of myoglobin molecules within the irradiated volume. To prepare the Mbmet sample, the buffer was exchanged by bidistilled water. The solution was freeze dried. For one sample, dry Mbmet was rehydrated by storing it in an atmosphere of high humidity until the water content reached the same amount as found in myoglobin crystals of the space group $P2_1$ ($h=0.38$ g H_2O/g protein). A CO ligated myoglobin sample was obtained by equilibrating a huge number of small deoxygenated myoglobin crystals in CO gas. The thickness of all samples was 14 mm. The ligation of the samples was controlled by optical spectroscopy and Mössbauer absorption spectroscopy. The humidity of the wet samples allows the comparison of the results with Mössbauer absorption [14] and inelastic neutron scattering [15]. At this humidity, translational diffusion of the whole protein molecules is suppressed but the protein specific dynamics is present [31].

Phonon-assisted Mössbauer absorption uses the fact that synchrotron radiation with an energy difference ε to the Mössbauer 14.413-keV level of ^{57}Fe can nevertheless be resonantly absorbed if phonons compensate the energy difference [26,27]. The deexcitation to the ground state occurs with the time delay τ_N of 141 ns by remission of γ quanta and by conversion electrons. Therefore, after irradiation with short x-ray pulses of synchrotron radiation, delayed quanta can be detected in a time resolving avalanche photodetector in between the synchrotron pulses [32]. The number of delayed quanta is a measure for the density of phonon states at the energy difference ε. The quanta that are promptly scattered by the electrons of the sample are discriminated by gating electronics.

The principal arrangement of the experiment is shown in Fig. 1. Pulsed x rays are produced by electron bunches circulating in a synchrotron storage ring crossing the alternating magnetic field of an undulator. The pulse length is typically 100 ps with a spacing depending on the actual bunch mode of the synchrotron. Within the $6+21*1$ mode at the APS the spacing is 153 ns, whereas it is 176 ns in the 16-bunch mode at the ESRF. A high heat load premonochromator of two diamond C(111) single crystals at the APS [two Si(111) single crystals at the ESRF] is delimiting the energy bandwidth to about 1 eV. The key part of the experimental setup is the high resolution monochromator, which reduces the energy bandwidth to the meV region [33]. Actually, the bandwidth was 4.4 meV for the deoxymyoglobin (Mbdeoxy) measured at the ESRF and 0.85 meV for measurements on Mbmet, MbCO, and one Mbdeoxy sample ($T=175$ K) at the APS. The hyperfine splitting of the Mössbauer level within the sample is of the order of 10 neV compared to the meV energy resolution of the monochromator. As a consequence, all hyperfine split levels are excited. The energy ε has been varied around the Mössbauer resonance level in steps of typically 0.28 meV by rotating the high resolution monochromator crystals [34]. A scan of $-80<\varepsilon<+80$ meV for one single phonon spectrum has taken typically 40 min. The loss in beam intensity due to the decreasing current in the storage ring during the scanning time has been taken into account by normalizing the measured intensities. In order to yield a spectrum of acceptable statistics 20–40 scans were added.

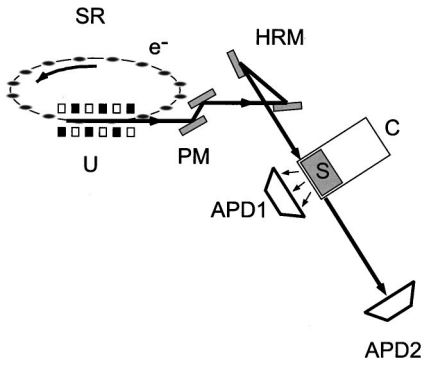

FIG. 1. Experimental setup for the phonon-assisted Mössbauer effect. The synchrotron storage ring SR (APS, Argonne or ESRF, Grenoble) is filled with electron bunches in a certain time structure. An undulator U produces x-ray pulses within the energy range of 14.413 keV with a bandwidth of about 380 eV. The bandwidth is further delimited to about 1 eV by a high heat load C(111)/C(111) or Si(111)/Si(111) premonochromator PM and to the meV regime by a tunable high resolution Si(975)/Si(975) monochromator HRM. The myoglobin samples S are situated within a closed cycle He cryostat C. The scattered radiation is detected by the avalanche photodiode APD1 whereas the forward scattered radiation is detected by APD2.

The detection of the radiation was done by an avalanche photodiode (APD1 in Fig. 1) [32] with a time resolution better than 1 ns. Both, the reemitted γ quanta of 14.413 keV and the *K*-fluorescence quanta of 6.4 keV were detected. Due to the internal conversion factor for ^{57}Fe, the higher efficiency of the detector for the lower energy and the multiple scattering of the resonant 14.413-keV photons, about 96% of the intensity came from the 6.4-keV radiation [35]. There-

fore, the method is incoherent and the re-emission takes place into the full solid angle. The APD1 has been situated as close as possible to the irradiated sample volume to cover a large solid angle. The energy resolution of the monochromator system was simultaneously measured by a second photodiode (APD2), which was situated in the forward direction far away from the sample (see Fig. 1). Due to the large distance, this detector counts only the elastic, coherent nuclear forward scattering of the ^{57}Fe of the sample. In some cases an additional iron foil was placed between the sample and the APD1 detector to increase the counting rate for the resolution measurement.

THEORY

We start with a theoretical normalized intensity spectrum $I(\varepsilon)$ including all elastic and inelastic scattering events. In practice, $I(\varepsilon)$ is the convolution of the normalized spectrum $S(\varepsilon)$ with the normalized energy resolution function $R(\varepsilon)$ of the spectrometer,

$$\int_{-\infty}^{\infty} I(\varepsilon)d\varepsilon = \int_{-\infty}^{\infty} R(\varepsilon)\otimes S(\varepsilon)d\varepsilon = 1. \tag{1}$$

In the case of harmonic vibrations, the spectrum can be assumed to consist of the elastic scattering $\delta(\varepsilon)$ and the inelastic scattering multiphonon terms $S_n(\varepsilon)$,

$$S(\varepsilon) = f\delta(\varepsilon) + f\sum_{n=1}^{\infty} S_n(\varepsilon). \tag{2}$$

f is the Lamb-Mössbauer factor, $f=\exp(-k^2\langle x^2\rangle)$ with $k=2\pi/\lambda$, and $\lambda=0.86$ Å in case of the ^{57}Fe radiation. The mean square displacement of the iron nucleus projected onto the direction of the incoming beam is denoted by $\langle x^2\rangle$. The energy difference to the Mössbauer resonance energy is ε.

The n-phonon scattering for $n\geqslant 2$ can iteratively be produced from the $(n-1)$-phonon term and the one-phonon term by convolution [36],

$$S_n = \frac{1}{n} S_1 \otimes S_{n-1}, \quad n\geqslant 2. \tag{3}$$

In order to get the contribution of the n-phonon scattering, we use the Fourier-logarithm method according to [27,37]. Combining Eq. (2) with Eq. (3) yields $S(\varepsilon)$ as a series of the single phonon scattering $S_1(\varepsilon)$. Each term S_n is derived from $S_1(\varepsilon)$, n times convoluted with itself, and divided by the factorial of n. Using the convolution theorem of Fourier transformation, one obtains the Taylor series of the exponential function of the Fourier transform of $S_1(\varepsilon)$

$$\exp[\mathcal{F}\{S_1(\varepsilon)\}] = \frac{\mathcal{F}\{R(\varepsilon)\otimes S(\varepsilon)\}}{f\mathcal{F}\{R(\varepsilon)\}} = \frac{1}{f}\mathcal{F}\{S(\varepsilon)\}, \tag{4}$$

$\mathcal{F}$ indicates the Fourier transform.

The density $D(\varepsilon)$ of phonons coupling to the iron is calculated from the one-phonon scattering by

$$D(\varepsilon) = \frac{\varepsilon}{E_R}[1-\exp(-\varepsilon/k_BT)]S_1(\varepsilon). \tag{5}$$

Equation (5) yields the density of phonon states without any further assumption apart from the condition that the vibrations are harmonic. $D(\varepsilon)$ calculated from the normalized scattering spectrum is also normalized.

For each vibrational mode of energy ε, the dynamical mean square displacement $\langle(\mathbf{k}\cdot\mathbf{r})^2/k^2\rangle=\langle r^2(\varepsilon)\rangle\cos^2(\varphi)$ of the iron atom in the direction of $\mathbf{k}$ can be calculated. Here φ is the angle between $\mathbf{k}$ and $\mathbf{r}$. The investigated powder and multicrystalline samples have a statistical distribution of the orientation of the myoglobin molecules to the incoming beam. Under this condition, $\frac{1}{3}$ of the quadratic amplitude of the harmonic vibration $\langle r^2(\varepsilon)\rangle=\langle x^2(\varepsilon)\rangle+\langle y^2(\varepsilon)\rangle+\langle z^2(\varepsilon)\rangle$ is obtained as the mean value over all directions. Assuming an isotropic behavior one has $\langle x^2(\varepsilon)\rangle=\langle y^2(\varepsilon)\rangle=\langle z^2(\varepsilon)\rangle=\frac{1}{3}\langle r^2(\varepsilon)\rangle$. The mean square displacement $\langle x^2(\varepsilon)\rangle$ coming from the vibration mode with the energy ε is given by [38]

$$\langle x^2(\varepsilon)\rangle = \frac{\hbar^2}{m_{\mathrm{Fe}}}\frac{D(\varepsilon)}{\varepsilon}\left(\frac{1}{\exp(\varepsilon/k_BT)-1}+\frac{1}{2}\right). \tag{6}$$

The isotropic mean square displacement $\langle x^2(0,\varepsilon)\rangle$ of the iron for all modes up to the energy ε can be calculated by the integration of $\langle x^2(\varepsilon)\rangle$.

$$\langle x^2(0,\varepsilon)\rangle = \frac{\hbar^2}{m_{\mathrm{FE}}}\int_0^{\varepsilon}\frac{D(\tilde{\varepsilon})}{\tilde{\varepsilon}}\left(\frac{1}{\exp(\tilde{\varepsilon}/k_BT)-1}+\frac{1}{2}\right)d\tilde{\varepsilon}. \tag{7}$$

The mean square displacement $\langle x^2\rangle$ as measured by the Lamb-Mössbauer factor is obtained by an integration from 0 to ∞.

EXPERIMENTAL RESULTS

Two conformations of sperm whale myoglobin can be distinguished by x-ray crystallography. In the t conformation (t denotes tensed) the sixth coordination of the iron atom is unoccupied whereas in the r conformation (r denotes relaxed) a ligand is bound. The t conformation is represented by Mbdeoxy. It is in the 2+ high spin state and has a domed heme, with the iron atom at about 0.4 Å out of the heme plane. In the r conformation of MbCO and Mbmet, the heme is more planar and the iron is close to the plane [9].

In the experiments Mbdeoxy, MbCO, and Mbmet have been investigated. A sample consisting of a large number of small Mbdeoxy crystals was measured at $T=295$, 189, 124, and 73 K with an energy resolution of 4.4 meV at ID18, ESRF and at $T=175$ K with 0.85 meV energy resolution at SRI-CAT-3ID, APS. The spectra obtained at the ESRF are shown in Fig. 2. The energy resolution function is given as a dashed line. The abscissa denotes the energy differences ε of the incoming synchrotron radiation to the Mössbauer level of ^{57}Fe. At positive energies vibrations are created in the resonance absorption process (Stokes), whereas at the negative side vibrations have to be annihilated during the absorption to gain the energy difference (anti-Stokes). The discrepancy

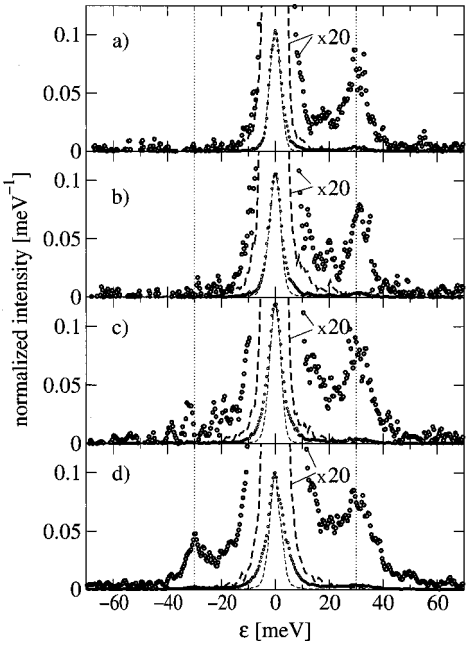

FIG. 2. Phonon spectra of deoxymyoglobin at $T=73$, 124, 189, and 295 K, pictures (a)–(d), respectively. The scaling is done by Lipkin's sum rule (see text). The same data are given enlarged by a factor of 20, respectively. Circles, complete inelastic and elastic scattering dependent on the energy difference ε to the Mössbauer resonance level of ^{57}Fe of 14.413 keV. Dashed line, resolution function $R(\varepsilon)$ of 4.4 meV FWHM. Dotted line, guide to the eye at ± 30 meV to mark a peak position in the inelastic scattering regime.

in intensity at both sides is known as the detailed balance. Figure 3 shows spectra of Mbdeoxy measured with the energy resolution of 4.4 and 0.85 meV, respectively. The improvement by the enhanced energy resolution is clearly seen. At the lowest energies, a step in the phonon spectrum can now be resolved from the elastic line.

Freeze dried Mbmet rehydrated to the same water content as found in myoglobin crystals ($h=0.38$ g H_2O/g protein)

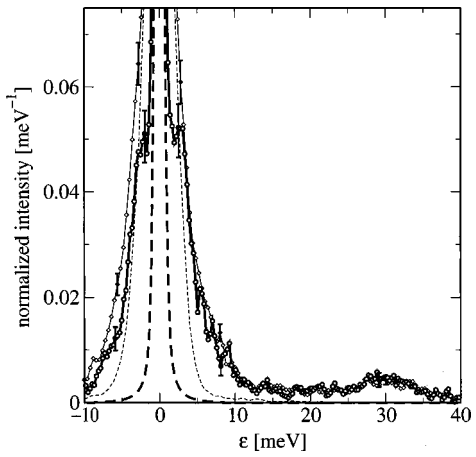

FIG. 3. Phonon spectra of deoxymyoglobin at 189 and 175 K. Diamonds, data obtained with 4.4-meV resolution; circles, data obtained with 0.85-meV resolution exposing additional features in the low energy regime. The respective resolution functions are given as dashed lines.

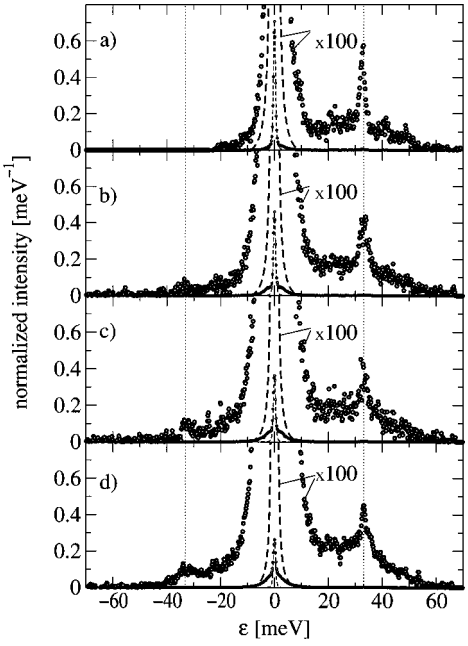

FIG. 4. Phonon spectra of metmyoglobin at 50, 170, 235, and 300 K denoted by (a)–(d). Data are normalized and enlarged by a factor of 100. Circles, complete inelastic and elastic scattering dependent on the energy difference ε to the Mössbauer resonance level of ^{57}Fe of 14.413 keV. Dashed line, resolution function $R(\varepsilon)$ of 0.85 meV FWHM. Dotted line, guide to the eye at ± 33 meV to mark a peak position in the inelastic scattering regime.

was measured at temperatures between 50 K and room temperature (compare Fig. 4). The spectra of Mbmet have one distinct maximum at about $\varepsilon=33$ meV (266 cm^{-1}) representing a well-defined vibration. The dotted line is a guide to the eye showing that the energy position of this vibration is not changing with temperature even at 300 K. This is a matter of fact for all samples investigated.

The spectra of freeze dried Mbmet were obtained at 304 and 168 K. In Fig. 5 the room temperature data of wet and dry Mbmet are compared. The density of the line at 33 meV present in the wet sample is diminished and two additional lines at 42 and 48 meV become visible leading to a broad shoulder between 35 and 50 meV.

The phonon spectra of MbCO crystals were recorded at 40 and 235 K. In addition a sample with a 1/1 mixture of MbCO and Mbdeoxy was examined at 42, 58, 165, and 240 K. As an example, Fig. 6(a) shows the phonon spectrum of pure MbCO at 40 K, Fig. 6(b) shows a spectrum of a 1/1 mixture of MbCO with Mbdeoxy at 42 K. The phonon spectrum of MbCO in Fig. 6(a) exhibits at least five resolved iron vibrations at 33, 40, 45, 64, and 73 meV. The modes at 30–33 meV are enhanced in Fig. 6(b) due to the additional Mbdeoxy as compared to Fig. 6(a).

DATA ANALYSIS

The spectra shown in Figs. 2–6 have to be analyzed by Eq. (4) to extract the one-phonon contribution S_1 and the higher contributions S_n using Eq. (3). Unfortunately, $S(\varepsilon)$ cannot be measured directly. A serious problem arises from

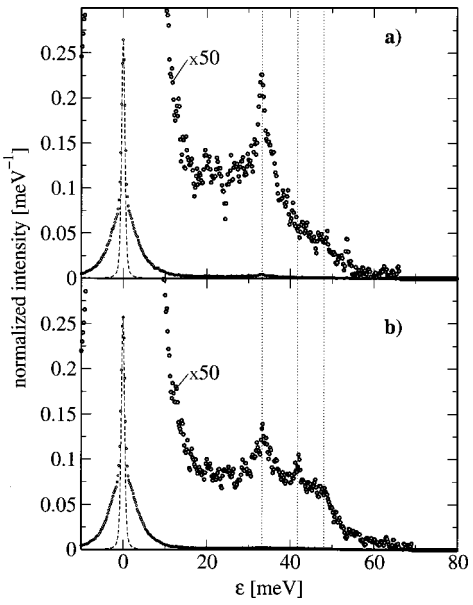

FIG. 5. Phonon spectra of wet (a) and dry (b) Mbmet at 300 K normalized and enlarged by a factor of 50. Circles, complete inelastic and elastic scattering dependent on the energy difference ε to the Mössbauer resonance level of ^{57}Fe of 14.413 keV. Dashed line, resolution function $R(\varepsilon)$ of 0.85 meV FWHM. Dotted lines, guide to the eye at 33, 42, and 48 meV to mark peak positions in the inelastic scattering regime. Whereas the peak at 33 meV scales down by going from wet to the dry myoglobin, the peaks at 42 and 48 meV are invisible in the wet sample.

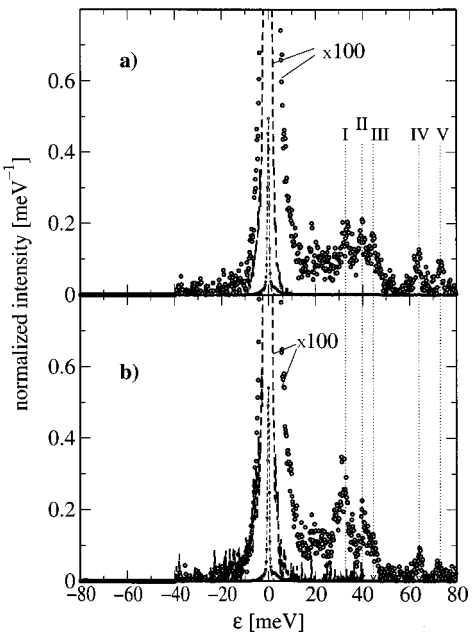

FIG. 6. Phonon spectra of pure MbCO (a) and a 1/1 mixture of MbCO with Mbdeoxy (b) at 40 and 42 K, respectively. Circles, complete inelastic and elastic scattering dependent on the energy difference ε to the Mössbauer resonance level of ^{57}Fe of 14.413 keV. Dashed line, resolution function $R(\varepsilon)$ of 0.85 meV FWHM. The data are given after scaling with Lipkin's sum rule and rescaled by a factor of 100. Five distinct peaks are named I–V and marked with dotted lines.

the energy dependence of the extinction of the incoming radiation within the sample. Off nuclear resonance, the incoming beam is only slightly weakened by electronic absorption. At nuclear resonance ($\varepsilon=0$), an additional strong Mössbauer absorption occurs. As a result, the elastically scattered intensity, measured in the experiment, is too small. In contrast, the nuclear forward scattered intensity at $\varepsilon=0$ may be scattered by the electrons of the atoms into APD1 and increase the elastically scattered intensity [39]. The experimentally obtained intensity spectrum becomes

$$I_{\mathrm{expt}}(\varepsilon)=cR(\varepsilon)\otimes S_{\mathrm{expt}}(\varepsilon) \tag{8}$$

with the energy spectrum

$$S_{\mathrm{expt}}(\varepsilon)=fa\,\delta(\varepsilon)+f\sum_{n=1}^{\infty}S_n(\varepsilon), \tag{9}$$

c is a normalization constant. The resolution functions $R(\varepsilon)$ shown in Figs. 2–6 as dashed lines have been measured in the direct beam by APD2. The factor a ($\neq 1$) takes into account the modification of the elastic intensity by extinction of the incoming beam due to Mössbauer absorption and the electronic scattering of the nuclear forward scattering. The experimentally obtained energy spectrum is correlated to $S(\varepsilon)$ by

$$S(\varepsilon)=S_{\mathrm{expt}}(\varepsilon)+f(1-a)\,\delta(\varepsilon)\,. \tag{10}$$

For a conversion of the experimental data we need the parameters c, f and a.

The normalization constant c can be derived by Lipkin's sum rule: The first moment of the normalized spectrum $S(\varepsilon)$ [see Eq. (2)] has to be equal to the recoil energy $E_R=1.956$ meV of a free ^{57}Fe nucleus emitting the Mössbauer radiation of $E=14.413$ keV [40–42]. For the first moment of the measured intensity one obtains

$$\begin{aligned}A&=\int_{-\infty}^{\infty}\varepsilon I_{\mathrm{expt}}(\varepsilon)d\varepsilon\\&=c\int_{-\infty}^{\infty}\varepsilon R(\varepsilon)\otimes S_{\mathrm{expt}}(\varepsilon)d\varepsilon\\&=c\int_{-\infty}^{\infty}\varepsilon S_{\mathrm{expt}}(\varepsilon)d\varepsilon\\&=c\int_{-\infty}^{\infty}\varepsilon\left\{fa\,\delta(\varepsilon)+f\sum_{n=1}^{\infty}S_n(\varepsilon)\right\}d\varepsilon\\&=cf\int_{-\infty}^{\infty}\varepsilon\sum_{n=1}^{\infty}S_n(\varepsilon)d\varepsilon=cE_R\,.\end{aligned} \tag{11}$$

$R(\varepsilon)$ is a symmetric function up to a good approximation. The part of the first moment of $R(\varepsilon)$ is of the order of 1% of E_R. Nevertheless the slight asymmetry of $R(\varepsilon)$ is taken into

account in the data analysis (see, e.g., [43]) but not explicitly given in the equations to simplify matters.

The integration over $d\varepsilon$ eliminates the contribution of all terms that are even in ε because of the multiplication with ε. The same is true for the elastic scattering; therefore, the factor a does not influence the result. In order to obtain A, a numerical integration of the experimentally obtained intensity spectrum with the weight factor ε for $I_{\mathrm{expt}}(\varepsilon)$ is necessary. Note, that this integration is performed over the whole spectrum including the elastic line since all symmetric contributions cancel. With this procedure $c=A/E_R$ and the normalization of the inelastic spectrum is done.

Due to this normalization the inelastic spectrum is absolutely determined outside the elastic line but the section under the elastic line is still vague. In the region $\varepsilon=0$, we still cannot separate the contribution of elastic and inelastic scattering. Since the δ function describing the elastic scattering is also convoluted with $R(\varepsilon)$, the elastic line is not sharp, and elastic and inelastic scatterings overlap. Without a knowledge of the energy dependence of the inelastic scattering including the multiphonon terms under the elastic line, a subtraction of an elastic fraction $f\,a\,R(\varepsilon)\otimes\delta(\varepsilon)$ and subsequent addition of the theoretical elastic part $fR(\varepsilon)\otimes\delta(\varepsilon)$ to reconstruct the intensity $I(\varepsilon)$ is questionable. This problem cannot be ignored since the low energy regime has a large influence on the vibrational features derived from the spectra. We solved the problem by an iterative procedure. In the first step we assume a reasonable value for the parameter a. Equation (12), derived from Eq. (10), states that this is equivalent to an assumption of the f factor, which can be taken from Mössbauer absorption experiments, if available.

$$\int_{-\infty}^{\infty} R(\varepsilon)\otimes S_{\mathrm{expt}}(\varepsilon)\,d\varepsilon = af+(1-f). \tag{12}$$

The left side in Eq. (12) is known from numerical integration of the normalized experimental data. It gives the sum of the inelastic and elastic scattering, where the elastic scattering is modified by the factor a. Hence the left side of Eq. (12) is yielded by the normalized experimental data, the absorption correction a and the Lamb-Mössbauer factor f are correlated.

The smallest possible value, $a=0$, means that the entire spectrum is assumed to be inelastic. The largest reasonable value for a is reached when the total central part of the spectrum is due to elastic scattering. If a is taken larger, the subtraction of the elastic intensity $f\,a\,R(\varepsilon)\otimes\delta(\varepsilon)$ from the spectrum gives negative values for the remaining inelastic intensity near the elastic line.

With an assumption of a we can calculate the phonon density spectrum from the normalized experimental spectrum according to Eqs. (4) and (5). To be concrete we give as an example the analysis of the Mbmet spectrum shown in Fig. 4(b) for $T=170$ K. Figure 7 shows the low energy phonon density obtained with different a or f values, respectively. The value $f=0.6$ would give a negative density of states below $\varepsilon=1$ meV and can be, therefore, excluded. A 2% change from $f=0.5$ to $f=0.49$ increases the calculated density of states by more than 10% below 1 meV, whereas the densities are indistinguishable above 3 meV.

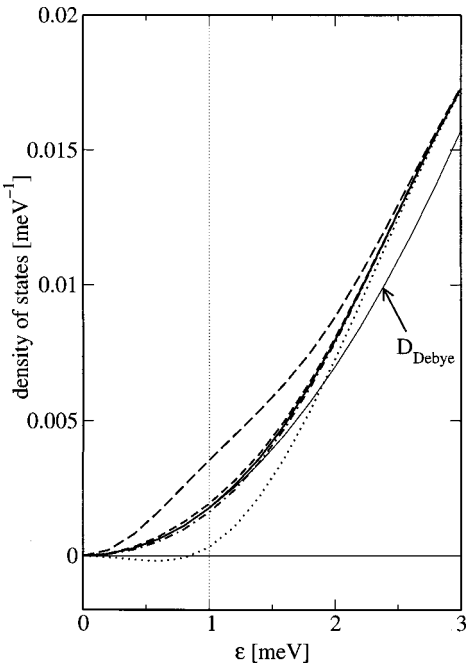

FIG. 7. The very low energy regime of the density of states $D(\varepsilon)$ of Mbmet at $T=170$ K. The density of states are calculated for different f values. The long-dashed, dashed, solid, dashed-dotted, and dotted lines are for $f=0.40$, 0.49, 0.50, 0.51, and 0.60, respectively, corresponding to $a=0.9800$, 0.9837, 0.9840, 0.9843, and 0.9867. A fit of a Debye density of states below $\varepsilon_{\mathrm{Bril}}=1$ meV to these curves shows that $f=0.50$ gives the best agreement with an ε^2 dependence (compare parabola D_{Debye}). The velocity of sound derived by Eq. (13) is $\overline{v_g}=1986\pm53$ m/s.

In the next step we improve the f value by assuming that the phonon density spectrum at very low energies up to an energy $\varepsilon_{\mathrm{Bril}}$ has to have a Debye behavior, i.e., it should follow the ε^2 law. One now has to estimate $\varepsilon_{\mathrm{Bril}}$. The sperm whale myoglobin crystals used in this investigation belong to the space group $P2_1$ with the unit cell parameters $a=64.5$, $b=30.9$, and $c=34.9$ Å, and $\beta=105.8°$ [3]. The unit cell includes two myoglobin molecules and about 800 water molecules. The protein has the shape of a flat ellipsoid of about $40\times40\times25$ Å^3. We can now estimate $\varepsilon_{\mathrm{Bril}}$ at the boundary of the first Brillouin zone. For that purpose we represent the unit cell by a sphere of equal volume, with the diameter d_{Bril}. The wave vector at the Brillouin boundary then becomes $K_{\mathrm{Bril}}=\pi/d_{\mathrm{Bril}}$, and $\varepsilon_{\mathrm{Bril}}$ is calculated by $\varepsilon_{\mathrm{Bril}}=v_g\hbar K_{\mathrm{Bril}}$ with $v_g=2000$ m/s [44,45]. The maximum energy for the acoustic branches should be about 0.8 meV. If the zone boundary is calculated not by the whole unit cell but by the asymmetric unit represented by one single myoglobin molecule, $\varepsilon_{\mathrm{Bril}}$ becomes 1 meV: Therefore, we analyzed which curve in Fig. 7 follows a Debye law $D_{\mathrm{Debye}}(\varepsilon)=d\varepsilon^2$ up to 1 meV with an arbitrary parameter d. The figure of merit was determined by the mean square deviation χ^2. $f=0.50$ gave the smallest deviation and was taken for the final analysis. At this point we can convert $S_{\mathrm{expt}}(\varepsilon)$ into $S(\varepsilon)$ using two parameters c and a or f. $D(\varepsilon)$ can then be calculated with Eqs. (3)–(5).

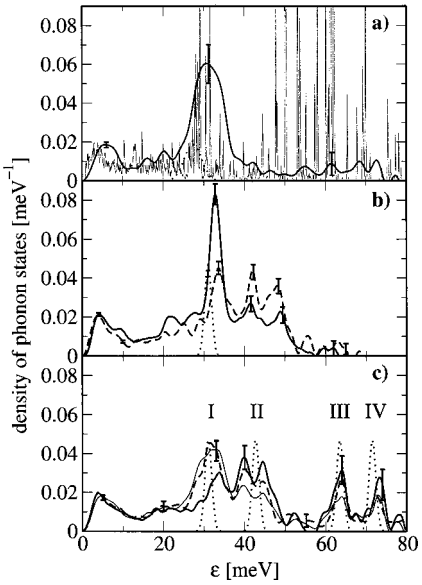

FIG. 8. Density of vibrational states, $D(\varepsilon)$, of myoglobin for different ligations. (a) Mbdeoxy averaged over $T=73$, 124, and 189 K, measured with an energy resolution of 4.4 meV and smoothed to an effective width of 5 meV for the presentation (see related text). Dotted line: Gaussian distribution with a maximum at the iron-histidine Raman line at 27.3 meV [71] and a full width of 5 meV. The gray line gives the density of normal mode vibrations of Mbdeoxy convoluted with a Gaussian distribution of 0.15 meV FWHM. (b) Thick solid line: wet Mbmet averaged over $T=50$, 170, and 235 K. Dashed line: dry Mbmet averaged over $T=145$ and 304 K. Both are measured with an energy resolution of 0.85 meV and smoothed to an effective width of 2 meV. Dotted line: Gaussian distribution with a maximum at the Raman line at 31.0 meV and a full width of 2 meV, assigned to an out-of-plane concerted pyrrole tilting mode including the Fe atom [72]. (c) Solid line: MbCO averaged over $T=40$ and 235 K, measured with an energy resolution of 0.85 meV and smoothed to an effective width of 2 meV. Dashed line: 1/1 mixture of MbCO and Mbdeoxy. Thin solid line: 1/1 weighted sum of the Mbdeoxy density of (a) and the MbCO density of (c). Dotted lines: Gaussian distributions with a maximum at the Raman lines, respectively, and a full width of 2 meV, (I) Raman line at 31.0 meV assigned to an out-of-plane concerted pyrrole tilting mode including the Fe atom [72], (II) iron in plane mode at 42.7 meV [73], (III) iron-CO stretching vibration at 63.5 meV [74], and (IV) iron-C-O bending vibration at 71.5 meV [74].

Figure 8 shows the result of the data analysis for Mbdeoxy, Mbmet, and MbCO. The density of states $D(\varepsilon)$ is independent of temperature above an energy of about 3 meV. Therefore the data were averaged over the temperatures for this presentation. The deconvolution of the data by the resolution function $R(\omega)$ during the procedure of the Fourier-logarithm decomposition [see Eq. (4)] is reversed for the data presented in Fig. 8 by convolution of the density of states for Mbdeoxy by a Gaussian of 5 meV FWHM and for Mbmet and MbCO by 2 meV FWHM, respectively. The error bars give the σ uncertainty and are obtained by error propagation from the statistical variation of the data.

In Figs. 9(a) and 9(b) we show some details for Mbmet at room temperature. Figure 9(a) gives the low energy regime of the phonon spectrum. Not only the one-phonon scattering

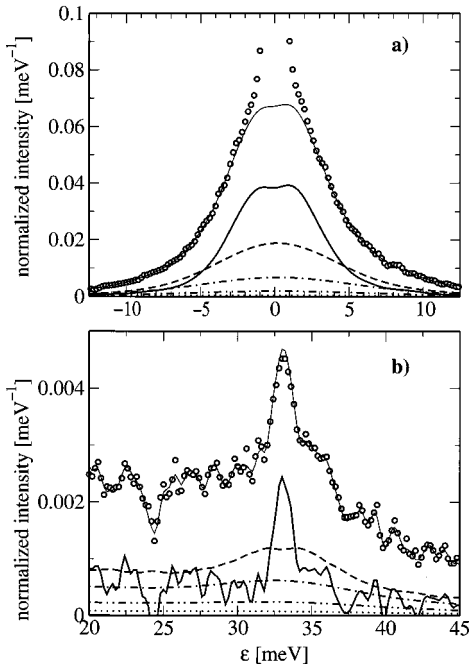

FIG. 9. Multiphonon contributions of metmyoglobin at 300 K in the low energy regime (a) and in the phonon creation regime (b). Open circles, phonon spectrum scaled by Lipkin's sum rule. Thin solid line, inelastic scattering contribution to the total spectrum. This contribution is the sum over the n-phonon scattering with n running from 1 to ∞. Thick solid line, one-phonon scattering. Dashed line, dashed-dotted, dashed double dotted, and dotted lines, two-, three-, four-, and five-phonon scattering contribution. The n-phonon parts in (a) are first deconvoluted by $R(\varepsilon)$ during the data analysis procedure and convoluted with a Gaussian of 2 meV FWHM for the presentation. In (b) the phonon scattering is deconvoluted by $R(\varepsilon)$ and convoluted with a Gaussian of 1 meV FWHM.

but also the two- and three-phonon scattering have a maximum at zero energy, which cannot be neglected. The total inelastic scattering is the sum over all multiphonon terms as $f\Sigma_{n=1}^{\infty}G(\varepsilon)\otimes S_n(\varepsilon)$ and is given as the thin solid line. In Fig. 9(b) a part of the higher energy regime is picked out to demonstrate that the multiphonon contribution plays a major role also at higher energies. $G(\varepsilon)$ is a Gaussian with 2 meV FWHM in Fig. 9(a) and 1 meV FWHM in Fig. 9(b) to smooth the extracted n-phonon contributions.

DISCUSSION

Data evaluation

In Fig. 4 it is shown that the energy of well-resolved vibrations in Mbmet is not changing with temperature up to 300 K. An analog behavior holds for all samples investigated. Therefore, it is experimentally verified that the harmonic low temperature dynamics is present also in the physiological temperature regime above 180 K. Moreover, it proves that the harmonic approach used for the analysis is valid. The harmonic behavior is also the basis for the application of the Fourier-logarithm deconvolution. This deconvolution also assumes that quasielastic contributions, if

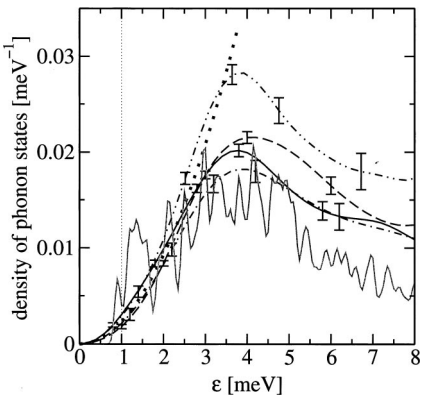

FIG. 10. Low energy density of phonon states for Mbmet, MbCO, and Mbdeoxy. Solid line, freeze dried Mbmet at 168 K; dashed line, freeze dried, rehydrated ($h=0.38$ g H_2O/g protein) Mbmet averaged over $T=170$ and 235 K; dashed dotted line, MbCO crystals ($h=0.38$ g H_2O/g protein) averaged over $T=40$ and 235 K; dashed double-dotted line, Mbdeoxy crystals ($h=0.38$ g H_2O/g protein) at $T=175$ K. The gray line gives the density of normal mode vibrations of MbCO convoluted with a Gaussian distribution of 0.15 meV FWHM. The thick dotted parabola line outlines the low energy regime of a Debye density of states. The vertical dotted line gives the estimated Brillouin zone boundary of myoglobin crystals. Note, that the good agreement of phonon densities at the iron with those from normal modes is limited to energies smaller than 3 meV.

present, are hidden by the resolution function of the experiment and are indistinguishable from elastic scattering. Nevertheless, we cannot use the data analysis described in the literature [46–48]. In this analysis one has to choose from the shape of the spectrum a phonon region in which the experimental data are interpolated by the dependence $S(\varepsilon) \propto \varepsilon/[1-\exp(-\varepsilon/k_BT)]$. In [46] this range was chosen as $-8 \leqslant \varepsilon \leqslant +8$ meV. In Mbmet (Fig. 4) an analogous choice would suggest the range $-20 \leqslant \varepsilon \leqslant +20$ meV. The spectrum shows no features that would allow the choice of a smaller interval. With this calibration, the phonon density would show a quadratic energy dependence up to 20 meV. We would obtain a sound velocity of 76 400 m/s, which makes no sense, and a Lamb-Mössbauer factor of $f=0.85$ at $T=170$ K in total contradiction to Mössbauer absorption experiments, which give $f=0.6$ as the upper limit at 170 K [12,49,50]. This way of data analysis assumes that only one-phonon processes are present. Our analysis shows that this is not the case. This is essential for soft material.

Figures 7 and 8 give clear evidence for a nearly quadratic increase of the density up to about 3 meV. Remarkably, the quadratic energy dependence continues into an energy regime, where the density should be determined by optical phonons. In Fig. 10 we compare the low energy part of the phonon density of Mbmet, MbCO, and Mbdeoxy. To get a better significance, temperature averages over 170 and 235 K have been used for wet Mbmet, over 40 and 235 K for MbCO, and for Mbdeoxy the high resolution data at 175 K are shown. All samples behave rather similar up to 3 meV. In addition, the phonon density calculated from normal modes is shown after convolution with a Gaussian of 0.15 meV FWHM. The normal mode analysis yields only optical phonons because it has been performed on one single molecule of myoglobin [22]. Nevertheless, this density is not too far away from a quadratic energy dependence between 1 and 3 meV. A value of $\varepsilon_{\mathrm{Bril}}$ between 0.8 and 1 meV corresponds to a minimum acoustic wavelength between 100 and 80 Å, respectively. An $\varepsilon_{\mathrm{Bril}}$ of 3 meV would correspond to an acoustic wave of only 27.5 Å, which is about the minor diameter of the protein molecule. For an explanation we have to remember that the forces between different molecules do not differ very much from those stabilizing the protein structure. Strong covalent bonds exist only along the linear polypeptide chain connecting the amino acids. The stabilization energy for both, the three-dimensional protein structure and the crystal, comes from hydrogen bridges, Coulomb interactions, van der Waals interactions, and hydrophobic interactions. The protein molecules in a crystal are in close contact at several positions. It is often difficult to see the borders between the different molecules in the electron density map. As long as the phonon wavelengths are large compared to the distance of atoms, the material can be treated in a continuum approach, well described by a Debye behavior.

Phonon-assisted Mössbauer effect allows the determination of the velocity of sound in proteins even at low temperatures and no crystals are needed. Within the Debye model one can calculate the velocity of sound according to [38],

$$D_{\mathrm{Debye}}(\varepsilon)=\frac{m_{\mathrm{Fe}}}{2\pi^2\rho\overline{v_g}^3\hbar^3}\varepsilon^2. \tag{13}$$

The density of myoglobin is $\rho=1.23$ g/cm^3 and the mass of the iron atom $m_{\mathrm{Fe}}=57\times1.66\times10^{-27}$ kg, $\overline{v_g}=[3v_t^3v_1^3/(2v_1^3+v_t^3)]^{1/3}$ is the mean velocity of sound, with v_1 and v_t being the longitudinal and transversal velocity, respectively. The bar above $\overline{v_g}$ denotes an additional average over all directions. The results are shown in Fig. 11. Only the ''real'' Debye modes below 1 meV are used.

The velocity of sound within proteins was scarcely yielded up to now. The present data for the mean velocity can be compared with those of the longitudinal sound velocity in hemoglobin (1828 m/s) and ribonuclease (1784 $\pm$72 m/s) yielded by laser-generated ultrasound measurements [44]. Coherent neutron scattering on dry *C*-pycocyanin yielded 2200 m/s [45].

The phonon density of different ligations of Mb

Here we make only some brief remarks concerning the energy regime between 4 and 80 meV. A detailed discussion of the density of states in the context of Raman lines and a normal mode analysis will be given elsewhere. The densities of states of Mbdeoxy, Mbmet, and MbCO are shown in Fig. 8. Different ligation states can be distinguished and the modes clearly change by drying out the protein [see Fig. 8(b)]. The position of some prominent Raman modes, given by broken lines in Fig. 8, do not necessarily coincide with maxima in the phonon density of states [29]. This matter of fact will be dealt with in a forthcoming paper.

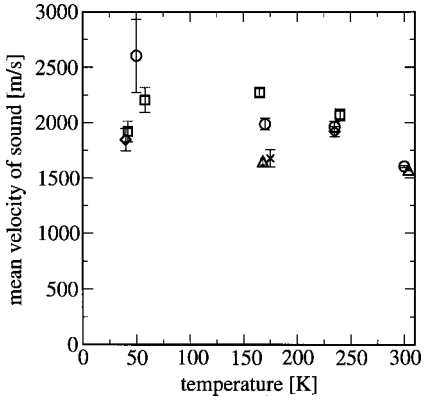

FIG. 11. The mean velocity of sound, $\overline{v_g}$, of the myoglobin samples obtained by assuming a Debye law given by Eq. (13) for the density of states below 1 meV. Circles, freeze dried, rehydrated ($h=0.38$ g H_2O/g protein) Mbmet at $T=50$, 170, 235, and 300 K. Squares, crystalline 1/1 mixture of MbCO and Mbdeoxy at $T=42$, 58, 165, and 240 K. Diamonds, crystalline MbCO at 40 and 235 K. Cross, crystalline Mbdeoxy at 175 K. Triangles, freeze dried Mbmet at 168 and 304 K.

Phonon densities obtained by incoherent scattering of neutrons

Incoherent neutron scattering yields the density of phonon states coupling to the hydrogen atoms of the protein [51]. A comparison of the hydrogen and the iron density of states can be done after a normalization with the respective masses. In Fig. 12 the hydrogen density of states divided by $m_H=1$ amu and the iron density divided by $m_{Fe}=57$ amu are compared. It has to be mentioned that neutron data give an average over all protons in the sample while phonon-assisted Mössbauer effect selects only displacements of the one iron atom in the molecule. Different modes contribute in the higher energy regime. The maximum in the hydrogen density at 60–80 meV is due to H_2O libration, that at 25–35 meV is due to CH_3 libration [51]. The mean square displacement of the heavy iron atom reaches that of the lightweight hydrogens at 33 meV. The concordance of both densities in the Debye regime below 1 meV is nearly perfect supporting again a continuum model in this energy regime.

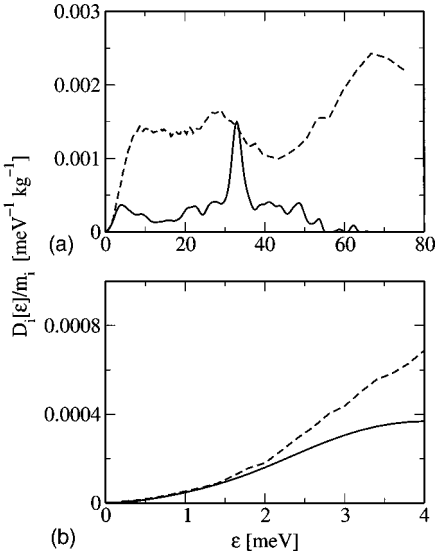

FIG. 12. Broken line: Hydrogen density of states D_H of Mbmet obtained by incoherent neutron scattering [51]. Solid line, iron density of states of Mbmet obtained by the phonon-assisted Mössbauer effect averaged over 50, 170, 235, and 300 K. To be comparable, the data are adjusted by m_H and m_{Fe}, respectively. (a) Complete energy regime, (b) low energy regime.

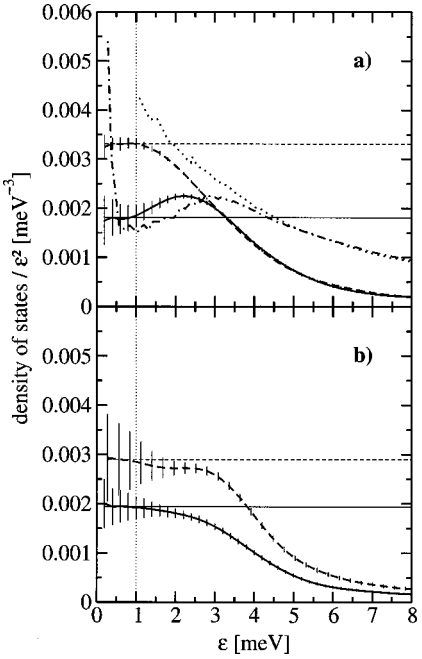

FIG. 13. The density of states $D(\varepsilon)$ of Mb scaled by $1/\varepsilon^2$ to focus on the deviation from the Debye density of states. (a) Thick solid line, $D(\varepsilon)/\varepsilon^2$ of freeze dried, rehydrated Mbmet as yielded by the phonon-assisted Mössbauer absorption at 235 K. Thick dashed line, $D(\varepsilon)/\varepsilon^2$ by phonon-assisted Mössbauer absorption at 300 K. Dashed dotted and dotted lines, $D(\varepsilon)/\varepsilon^2$ by incoherent neutron scattering [15] at 180 and 300 K, respectively. The Debye density of states for a sound velocity of 1962 m/s for 235 K and 1605 m/s for 300 K is shown as thin solid and dashed lines respectively. (b) $D(\varepsilon)/\varepsilon^2$ of crystalline samples of Mb show no enhancement above the Debye density of states. Thick solid line and thick dashed line, exemplary $D(\varepsilon)/\varepsilon^2$ of crystalline samples of MbCO at 235 K and deoxyMb at 175 K. The Debye density of states for a sound velocity of 1919 m/s for MbCO at 235 K and 1678 m/s for deoxyMb at 175 K is shown as thin solid and dashed lines, respectively.

The boson peak

Neutron scattering experiments as well as Raman scattering reveal an excess of vibrational modes over the Debye density in the low energy regime in glasses as well as proteins [15,52–55]. The physical nature of this so-called boson peak is still under discussion [52,56,57].

Figure 13(a) analyzes the result of the phonon-assisted Mössbauer absorption for the 235 K and the room temperature measurement of freeze dried, rehydrated Mbmet in more detail. The density is scaled as $D(\varepsilon)/\varepsilon^2$. In this way deviations from the Debye law are clearly seen. Such a deviation occurs for the 235-K data between 1 and 3 meV (similar

results are found for the data at 170 and 50 K). It could be interpreted as a boson peak. For comparison, $D(\varepsilon)/\varepsilon^2$ corresponding to a sound velocity of 1962 m/s [compare Fig. 13(a)] is shown. The dashed line is the result of the measurement at 300 K where an increase in the density of states in the low energy regime (see below) has already covered the tiny boson peak. The results of a neutron measurement on myoglobin at 180 and 300 K are given for comparison [15]. The results of both methods are rather similar. Only the boson peak is shifted from about 3 meV for the hydrogen atoms to about 2–2.5 meV for the iron atom at 235 K. This shift might be due to the overlaying effect of a mode softening (see below), which moves the apparent maximum in the $D(\varepsilon)/\varepsilon^2$ representation from 2.7 to 2.4 meV to 2.2 meV for 50, 170, and 235 K, respectively.

It has to be emphasized that no excess of modes could be measured with statistical significance in the crystalline samples. This is exemplary shown in Fig. 13(b) for crystals of MbCO at 235 K and deoxyMb at 175 K. The same behavior can by found for the glassy and crystalline states in glass-forming materials [58,59]. The exception of a boson peak in the crystalline state of tri-O-methyl-β-cyclodextrin was attributed to the influence of disordered regions in the crystalline state [60]. Nevertheless, though the disorder due to the distribution of an ensemble of myoglobin molecules among the conformational substates is evident, e.g., in the temperature dependent x-ray structure determination of myoglobin [3], this intramolecular disorder is not sufficient to result in a boson peak if this disordered structure is in a crystalline environment. We notice that this finding is at variance with recent molecular dynamics simulations, producing a boson peak of 230 water molecules surrounding one single molecule of plastocyanin [61], and disagrees also with a crystal simulation of ribonuclease *A* [62]. Neutron scattering also yields an excess of modes for freeze dried myoglobin, hence the maximum is shifted to lower energies in this case [63]. The same is found in molecular dynamics simulations on ribonuclease A [64]. However, this feature is not obtained by the phonon-assisted Mössbauer effect on the dry Mbmet sample probably due to the fact that a shift of the iron boson peak from 2–2.5 meV to still lower energies cannot be energetically resolved with the present resolution of the phonon-assisted Mössbauer effect.

Mean square displacements

With $D(\varepsilon)$ we are able to calculate mean square displacements as a function of the excited phonon modes according to Eq. (7). The result is given in Fig. 14 for MbCO at 300 K. We can now separate the contributions to the mean square displacements as shown in Fig. 14(b). The lower dashed part is the contribution to the $\langle x^2\rangle$ values due to the acoustic phonon branch with energies below 1 meV. These motions can already be excited at temperatures larger than 10 K. Their contribution to the total mean square displacements is about 25% at room temperature. The upper dashed part gives the $\langle x^2\rangle$ values due to the modes between 1 and 3 meV. About 40% of the total $\langle x^2\rangle$ is originated by these low energy modes, which follow the Debye law of an elastic medium. Since the myoglobin molecules with different ligations have a very similar phonon density in the low energy regime, the mean square displacements of molecules with different ligands are rather similar. The remaining $\langle x^2\rangle$ comes from well-defined optical modes. For comparison we also show the mean square displacement of the iron atom in MbCO calculated from the density of states of a normal mode analysis [22]. Modes with an energy above 10 meV contribute only slightly to the total mean square displacements. The total $\langle x^2\rangle$ values obtained by both methods coincide very well. Due to the nature of the normal modes calculated for one molecule, they start at about 1 meV where the acoustic phonons caused by the entire lattice end. The subsequent energy regime can already be interpreted by normal modes as seen in Fig. 10 for the density and in Fig. 14(a) for the resulting $\langle x^2\rangle$. Despite the good coincidence of the low energy regime of the density of states obtained by a normal mode analysis and the present experiment, it should be mentioned that the total normal mode mean square displacement is at least overestimated by about 25%. The loss of the modes in the Debye regime that cannot be calculated on one single molecule is compensated by additional modes between about 1 and 1.8 meV by the normal mode method (see Fig. 10). A similar problem arising for molecular dynamics simulations seems to be solved recently by introducing periodic boundary conditions [64–66]. Figure 8 demonstrates that the optical modes between 30 and 40 meV calculated by the normal mode analysis coincide well for Mbdeoxy [22],

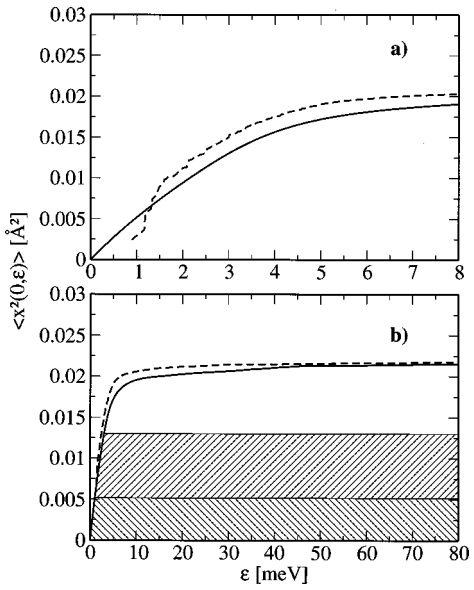

FIG. 14. Partial mean square displacement $\langle x^2\rangle$ of the iron atom in MbCO from the phonon-assisted Mössbauer absorption (solid line) and from a normal mode analysis (dashed line) [22] calculated as a function of the contributing modes at 300 K. At the abscissa value ε all modes between $\varepsilon=0$ and ε are taken into account. (a) The low energy regime. (b) The complete energy regime as covered by the phonon-assisted Mössbauer absorption. Lower dashed area, mean square displacement due to the acoustic phonon branch with energies below 1 meV. Upper dashed area, mean square displacement due to the modes between 1 and 3 meV.

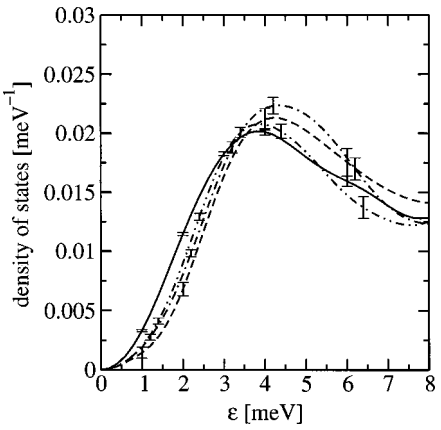

FIG. 15. Comparison of the density of phonon states at low energies for Mbmet. Dashed, dashed-dotted, and dashed double-dotted lines give the phonon densities at 50, 170, and 235 K, respectively, the solid line that at 300 K.

but the calculated modes at higher energies are less well represented in the measurement.

The low temperature and the high temperature regime in proteins, the physics of protein dynamics

Mössbauer absorption spectroscopy [5], flash photolysis experiments [4,67], as well as x-ray structure analysis [10] suggest to differentiate two temperature regimes. Below the so-called dynamical transition temperature T_{dyn}, a protein like myoglobin can no longer fulfill its function. Nevertheless, a huge number of special properties exist, characteristic for complex systems. In the physiological regime, above T_{dyn}, the protein is functional active, with a temperature depending rate. This scheme becomes not so obvious in the present investigations. This is discussed in Fig. 15. Below 3 meV the densities at 50, 170, and 235 K nearly coincide. In the physiological regime at $T=300$ K an increase of $D(\varepsilon)$ in the low energy region can be seen. It is not reasonable to explain this increase of phonon density by the presence of quasielastic motions coupling to the iron. A quasielastic line broadening was found by Mössbauer absorption experiments in the temperature regime above 180 K [14]. The energy transfer was of the order of 10–100 neV; quantized phonons no longer make any sense. It is proven by Mössbauer absorption, that the overall mean square displacement $\langle x^2\rangle$ of the iron is entirely determined by the harmonic vibrations and this neV dynamics excited above 180 K [6]. In the present experiments this neV energy transfer is totally covered by the ''elastic'' line of meV width. Therefore, a mechanism of mode softening is very probable. Due to small structural relaxations of the molecules in the physiological temperature regime some vibrational frequencies become ''softer.'' The density of low energy modes increases at the costs of higher frequencies. The influence of a mode softening can just be seen in the small increase of the density of states below 3 meV going from 50 to 170 K and 235 K before the density makes a large increase to 300 K.

Figure 16 shows the resulting mean square displacements as a function of temperature calculated from $D(\varepsilon)$ for Mbmet as stated by Eq. (7). $D(\varepsilon)$ was averaged over the densities yield for 50, 170, and 235 K. The integration was done over the measured energy regime from 0 to 80 meV. The low temperature $\langle x^2\rangle$ values are in good agreement with the Mössbauer absorption data [50,68]. The value at 235 K lies on the linear extrapolation of the low temperature Mössbauer mean square displacements. Only the 300 K $\langle x^2\rangle$ value is slightly above this extrapolated line. The phonon-assisted Mössbauer effect with meV energy resolution is not sensitive to the protein specific quasidiffusive modes, which cause the strong increase of the $\langle x^2\rangle$ values above 200 K determined by Mössbauer absorption spectroscopy. We miss this feature in the phonon-assisted Mössbauer effect.

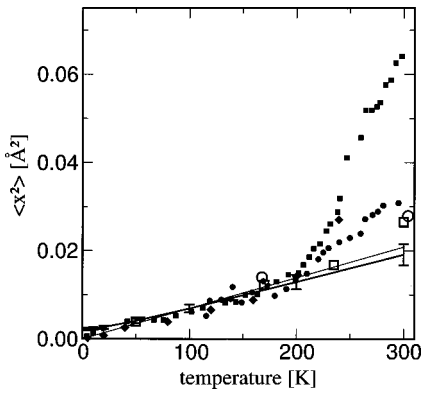

FIG. 16. Temperature dependence of the mean square displacement of the iron atom in myoglobin. Filled squares and filled diamonds, Mössbauer absorption measurements of Mbdeoxy by Parak, Knapp, and Kucheida [14] and of Mbmet by Steyer and Parak [50], respectively; open squares, phonon-assisted Mössbauer absorption of wet Mbmet, thick solid line, mean square displacement of the iron in Mbmet calculated from the density of states averaged over 50, 170, and 235 K [see Eq. (7)] Thin solid line, linear extrapolation of the low temperature slope of $\langle x^2\rangle$ from the Mössbauer absorption experiment of Parak, Knapp, and Kucheida [14]. Filled circles and open circles, Mössbauer absorption [70] and phonon-assisted Mössbauer effect at freeze dried Mbmet, respectively.

The comparison of the results of phonon-assisted Mössbauer effect and Mössbauer absorption spectroscopy gives a further insight into the physics of protein dynamics. A molecule of N atoms has $3N$-6 internal modes of motions. Mean square displacements are essentially determined by the low frequency modes (compare Fig. 14). Mössbauer absorption and phonon-assisted Mössbauer effect show that below T_{dyn} these modes are essentially harmonic. The results of phonon-assisted Mössbauer effect above T_{dyn} show that most of these harmonic motions are still present in the physiological temperature regime. Mode softening gives a small increase of the mean square displacement. The quasidiffusive motions seen in the Mössbauer absorption spectroscopy above T_{dyn} have to take some motional freedoms from the harmonic motions. A comparison with the phonon-assisted Mössbauer effect shows that only rather few degrees of freedom have to change their nature. This is in principal agreement with the theoretical calculations of Kitao and Go [69].

In Fig. 16 also the Mössbauer absorption results for dry Mbmet [70] are given. Whereas the density of states of the

dry sample at 168 K coincides well with the low temperature results of the wet protein, the density in the low energy regime of the dry protein at 304 K coincides well with that of the wet sample. In addition, one has to pay attention to the slight increase of the $\langle x^2 \rangle$ of the dry sample above the harmonic behavior at high temperatures. One may speculate that mode softening occurs also in the dry protein at physiological temperatures while the quasidiffusive motions need a hydration shell, which probably ensures a permanent exchange with water molecules within the protein moiety.

CONCLUSIONS

The density of states of dynamical modes coupling to the iron atom in myoglobin was obtained by the phonon-assisted Mössbauer effect. Whereas the position of optical modes coupling to the iron could be determined already by the inelastic scattering spectrum at low temperatures [28,29], detailed physical information can only be obtained by a precise extraction of the density of states. The data analysis allowed us to determine the density of states below the elastic scattering peak. This is of great importance for the understanding of the physical nature of the mean square displacement of the iron. It becomes possible to decompose the $\langle x^2 \rangle$ values into energy dependent portions $\langle x^2(\varepsilon) \rangle$. It was experimentally verified that most of the modes within the meV energy region stay harmonic in the physiological temperature regime. Mode softening occurs in the low energy regime at physiological temperatures. Our results may stimulate further theoretical investigations in the field of molecular dynamics investigations and normal mode analysis.

ACKNOWLEDGMENT

This work was supported by the Federal Ministry of Education and Research (BMBF) under Grant No. 05 SK8WOC 8.

[1] J. C. Kendrew, R. E. Dickerson, B. E. Strandberg, R. G. Hart, D. R. Davies, D. C. Phillips, and V. C. Shore, Nature (London) **185**, 422 (1960).
[2] H. Frauenfelder, G. A. Petsko, and D. Tsernoglou, Nature (London) **280**, 558 (1979).
[3] F. Parak, H. Hartmann, K. D. Aumann, H. Reuscher, G. Rennekamp, H. Bartunik, and W. Steigemann, Eur. Biophys. J. **15**, 237 (1987).
[4] R. H. Austin, K. W. Beeson, L. Eisenstein, H. Frauenfelder, and I. C. Gunsalus, Biochemistry **14**, 5355 (1975).
[5] F. Parak, A. Ostermann, A. Gassmann, C. Scherk, S.-H. Chong, A. Kidera, and N. Go, *Biological Physics: Third International Sympopsium*, edited by H. Frauenfelder, G. Hummer, and R. Garcia (AIP, New York, 1999), p. 117.
[6] S.-H. Chong, Y. Joti, A. Kidera, N. Go, A. Ostermann, A. Gassmann, and F. G. Parak, Eur. Biophys. J. **30**, 319 (2001).
[7] I. Schlichting, J. Berendzen, G. N. J. Phillips, and R. M. Sweet, Nature (London) **371**, 808 (1994).
[8] T. Y. Teng, V. Srajer, and K. Moffat, Nat. Struct. Biol. **1**, 701 (1994).
[9] H. Hartmann, S. Zinser, P. Komninos, R. T. Schneider, G. U. Nienhaus, and F. Parak, Proc. Natl. Acad. Sci. U.S.A. **93**, 7013 (1996).
[10] A. Ostermann, R. Waschipky, F. G. Parak, and G. U. Nienhaus, Nature (London) **404**, 205 (2000).
[11] V. Srajer, T. Teng, T. Ursby, C. Pradervand, Z. Ren, S. Adachi, W. Schildkamp, D. Bourgeois, M. Wulff, and K. Moffat, Science **274**, 1726 (1996).
[12] F. Parak and H. Formanek, Acta Crystallogr., Sect. A: Cryst. Phys., Diffr., Theor. Gen. Crystallogr. **27**, 573 (1971).
[13] H. Keller and P. G. Debrunner, Phys. Rev. Lett. **45**, 68 (1980).
[14] F. Parak, E. W. Knapp, and D. Kucheida, J. Mol. Biol. **161**, 177 (1982).
[15] S. Cusack and W. Doster, Biophys. J. **58**, 243 (1990).
[16] N. Go, T. Noguti, and T. Nishikawa, Proc. Natl. Acad. Sci. U.S.A. **80**, 3696 (1983).
[17] J. C. Smith, Q. Rev. Biophys. **24**, 227 (1991).
[18] S. Hayward, A. Kitao, and N. Go, Proteins: Struct., Funct., Genet. **23**, 177 (1995).
[19] K. Kuczera, J. Kuriyan, and M. Karplus, J. Mol. Biol. **213**, 351 (1990).
[20] J. C. Smith, K. Kuczera, and M. Karplus, Proc. Natl. Acad. Sci. U.S.A. **87**, 1601 (1989).
[21] B. R. Brooks and M. Karplus, Proc. Natl. Acad. Sci. U.S.A. **80**, 6571 (1983).
[22] B. Melchers, E. W. Knapp, F. Parak, L. Cordone, A. Cupane, and M. Leone, Biophys. J. **70**, 2092 (1996).
[23] E. Gerdau, R. Rüffer, H. Winkler, W. Tolksdorf, C. P. Klages, and J. P. Hannon, Phys. Rev. Lett. **54**, 835 (1985).
[24] J. B. Hastings, D. P. Siddons, U. van Bürck, R. Hollatz, and U. Bergmann, Phys. Rev. Lett. **66**, 770 (1991).
[25] C. Keppler, K. Achterhold, A. Ostermann, U. van Bürck, A. I. Chumakov, R. Rüffer, W. Sturhahn, E. E. Alp, and F. G. Parak, Eur. Biophys. J. **29**, 146 (2000).
[26] M. Seto, Y. Yoda, S. Kikuta, X. W. Zhang, and M. Ando, Phys. Rev. Lett. **74**, 3828 (1995).
[27] W. Sturhahn, T. S. Toellner, E. E. Alp, X. Zhang, M. Ando, Y. Yoda, S. Kikuta, M. Seto, C. W. Kimball, and B. Dabrowski, Phys. Rev. Lett. **74**, 3832 (1995).
[28] C. Keppler, K. Achterhold, A. Ostermann, U. van Bürck, W. Potzel, A. I. Chumakov, A. Q. R. Baron, R. Rüffer, and F. Parak, Eur. Biophys. J. **25**, 221 (1997).
[29] J. T. Sage, S. M. Durbin, W. Sturhahn, D. C. Wharton, P. M. Champion, P. Hession, J. Sutter, and E. E. Alp, Phys. Rev. Lett. **86**, 4966 (2001).
[30] F. W J. Teale, Biochim. Biophys. Acta **35**, 543 (1959).
[31] W. Doster, T. Kleinert, F. Post, and M. Settles, in *Protein-Solvent Interactions*, edited by R. B. Gregory (Dekker, New York, 1995).
[32] A. Q. R. Baron, Nucl. Instrum. Methods Phys. Res. A **352**, 665 (1995).
[33] T. S. Toellner, Hyperfine Interact. **125**, 3 (2000).

[34] T. S. Toellner, M. Y. Hu, W. Sturhahn, K. Quast, and E. E. Alp, Appl. Phys. Lett. **71**, 2112 (1997).
[35] A. I. Chumakov, J. Metge, A. Q. R. Baron, R. Rüffer, Y. V. Shvyd'ko, H. Grünsteudel, and H. F. Grünsteudel, Phys. Rev. B **56**, R8455 (1997).
[36] K. S. Singwi and A. Sjölander, Phys. Rev. **120**, 1093 (1960).
[37] D. W. Johnson and J. C. H. Spence, J. Phys. D **7**, 771 (1974).
[38] A. A. Maradudin, E. W. Montroll, and G. H. Weiss, in *Theory of Lattice Dynamics in the Harmonic Approximation*, edited by F. Seitz and D. Turnball, Solid State Phyics Vol. 3 (Academic, New York, 1963).
[39] A. I. Chumakov and W. Sturhahn, Hyperfine Interact. **123/124**, 781 (1999).
[40] H. J. Lipkin, Ann. Phys. **9**, 332 (1960).
[41] S. W. Lovesey, in *Theory of Neutron Scattering from Condensed Matter*, edited by R. J. Elliott, J. A. Krumhansl, W. Marshall, and D. H. Wilkinson, Nuclear Scattering Vol. 1 (Clarendon, Oxford, 1984).
[42] H. J. Lipkin, Phys. Rev. B **52**, 10 073 (1995).
[43] M. Y. Hu, W. Sturhahn, T. S. Toellner, P. M. Hession, J. P. Sutter, and E. E. Alp, Nucl. Instrum. Methods Phys. Res. A **428**, 551 (1999).
[44] C. Edwards, S. B. Palmer, P. Emsley, J. R. Helliwell, I. D. Glover, G. W. Harris, and D. S. Moss, Acta Crystallogr., Sect. A: Found. Crystallogr. **46**, 315 (1990).
[45] M.-C. Bellissent-Funel, J. Teixeira, S. H. Chen, B. Dorner, H. D. Middendorf, and H. L. Crespi, Biophys. J. **56**, 713 (1989).
[46] A. I. Chumakov, R. Rüffer, A. Q. R. Baron, H. Grünsteudel, and H. F. Grünsteudel, Phys. Rev. B **54**, R9596 (1996).
[47] V. G. Kohn, A. I. Chumakov, and R. Rüffer, Phys. Rev. B **58**, 8437 (1998).
[48] W. Sturhahn, Hyperfine Interact. **125**, 149 (2000).
[49] F. Parak, E. N. Frolov, R. L. Mössbauer, and V. I. Goldanskii, J. Mol. Biol. **145**, 825 (1981).
[50] J. Steyer and F. G. Parak (unpublished).
[51] M. Settles and W. Doster, in *Biological Macromolecular Dynamics*, edited by S. Cusack, H. Büttner, M. Ferrand, P. Langan, and P. Timmins (Adenine, New York, 1997), p. 3.
[52] M. Kataoka, H. Kamikubo, J. Yunoki, F. Tokunaga, T. Kanaya, Y. Izumi, and K. Shibata, J. Phys. Chem. Solids **60**, 1285 (1999).
[53] H. Urabe, Y. Sugawara, M. Ataka, and A. Rupprecht, Biophys. J. **74**, 1533 (1998).
[54] K. G. Brown, S. C. Erfurth, E. W. Small, and W. L. Peticolas, Proc. Natl. Acad. Sci. U.S.A. **69**, 1467 (1972).
[55] P. C. Painter, L. E. Mosher, and C. Rhoads, Biopolymers **21**, 1469 (1982).
[56] W. Schirmacher, G. Diezemann, and C. Ganter, Phys. Rev. Lett. **81**, 136 (1998).
[57] E. Courtens, M. Foret, B. Hehlen, and R. Vacher, Solid State Commun. **117**, 187 (2001).
[58] B. Frick, J. Williams, S. Trevino, and R. Erwin, Physica B **213&214**, 506 (1995).
[59] A. Tölle, H. Zimmermann, F. Fujara, W. Petry, W. Schmidt, H. Schober, and J. Wuttke, Eur. Phys. J. B **16**, 73 (2000).
[60] I. Tsukushia, T. Kanayaa, O. Yamamurob, T. Matsuob, and K. Kajia, J. Phys. Chem. Solids **60**, 1545 (1999).
[61] A. R. Bizzarri, A. Paciaroni, and S. Cannistraro, Phys. Rev. E **62**, 3991 (2000).
[62] M. Tarek and D. J. Tobias, Biophys. J. **79**, 3244 (2000).
[63] H. Leyser, W. Doster, and M. Diehl, Phys. Rev. Lett. **82**, 2987 (1999).
[64] M. Tarek and D. J. Tobias, J. Chem. Phys. **115**, 1607 (2001).
[65] M. Tarek and D. J. Tobias, J. Am. Chem. Soc. **121**, 9740 (1999).
[66] M. Tarek, G. J. Martyna, and D. J. Tobias, J. Am. Chem. Soc. **122**, 10 450 (2000).
[67] P. J. Steinbach, A. Ansari, J. Berendzen, D. Braunstein, K. Chu, B. R. Cowen, D. Ehrenstein, H. Frauenfelder, J. B. Johnson, D. C. Lamb, S. Luck, J. R. Mourant, G. U. Nienhaus, P. Ormos, R. Philipp, A. Xie, and R. D. Young, Biochemistry **30**, 3988 (1991).
[68] E. R. Bauminger, S. G. Cohen, I. Nowik, S. Ofer, and J. Yariv, Proc. Natl. Acad. Sci. U.S.A. **80**, 736 (1983).
[69] A. Kitao and N. Go, Curr. Opin. Struct. Biol. **9**, 164 (1999).
[70] F. Parak, M. Fischer, E. Graffweg, and H. Formanek, in *Structure and Dynamics of Nucleic Acids, Proteins and Membranes*, edited by E. Clementi and S. Chin (Plenum, New York, 1986), p. 139.
[71] P. V. Argade, M. Sassaroli, D. L. Rousseau, T. Inubishi, M. Ikeda-Saito, and A. Lapidot, J. Am. Chem. Soc. **106**, 6593 (1984).
[72] A. V. Wells, J. T. Sage, D. Morikis, P. M. Champion, M. L. Chiu, and S. G. Sligar, J. Am. Chem. Soc. **113**, 9655 (1991).
[73] S. Hu, K. M. Smith, and T. G. Spiro, J. Am. Chem. Soc. **118**, 12 638 (1996).
[74] M. Tsubaki, R. B. Srivastava, and N.-T. Yu, Biochemistry **21**, 1132 (1982).